

# Formation of $\text{Al}_2\text{O}_3\text{-Ta}_2\text{O}_5$ Double-Oxide Thin Films by Low-Pressure MOCVD and Evaluation of Their Corrosion Resistances in Acid and Alkali Solutions

Nobuyoshi Hara,\* Shintaro Nagata, Noboru Akao, and Katsuhisa Sugimoto\*

Department of Metallurgy, Graduate School of Engineering, Tohoku University, Sendai 980-8579, Japan

$\text{Al}_2\text{O}_3\text{-Ta}_2\text{O}_5$  double-oxide thin films with different cationic mole fractions of Ta,  $X_{\text{Ta}}$ , were formed by metallorganic chemical vapor deposition using aluminum tetraisopropoxide [ $\text{Al}(\text{O}-i\text{-C}_3\text{H}_7)_3$ ] and tantalum pentametoxide [ $\text{Ta}(\text{OCH}_3)_5$ ] as source gases and oxygen as a reaction gas. The corrosion resistances of the films were examined in 6 and 12 M HCl and 1 M NaOH at 298 K by the ellipsometric measurement of thinning rates of the films. The  $\text{Al}_2\text{O}_3\text{-Ta}_2\text{O}_5$  films having  $X_{\text{Ta}}$  values between 0.0 and 1.0 showed homogeneous amorphous structures. The thinning rate of the films in HCl solutions decreased with increasing  $X_{\text{Ta}}$  value and reached the analytical limit of ellipsometry. The films with  $X_{\text{Ta}}$  values larger than 0.35 hardly dissolved in 6 M HCl and those with  $X_{\text{Ta}}$  values larger than 0.45 in 12 M HCl. The corrosion resistance of the  $\text{Al}_2\text{O}_3\text{-Ta}_2\text{O}_5$  films in 1 M NaOH increased significantly with an increase in  $X_{\text{Ta}}$ : the dissolution rate of the  $\text{Al}_2\text{O}_3\text{-Ta}_2\text{O}_5$  film with  $X_{\text{Ta}}$  value of about 0.5 is lower than that of pure  $\text{Al}_2\text{O}_3$  film by six orders of magnitude.

© 1999 The Electrochemical Society. S0013-4651(98)04-098-1. All rights reserved.

Manuscript submitted April 29, 1998; revised manuscript received October 16, 1998.

In an earlier series of papers, thin films of double oxides having two or more different kinds of cations were synthesized by metallorganic chemical vapor deposition (MOCVD) and utilized as artificial passivation films for comparison to passive films formed on corrosion-resistant alloys.<sup>1-9</sup> Since the artificial passive films are prepared on an inert substrate, it is possible to elucidate the quantitative relationship between the corrosion resistance and the composition of the films without any influence of substrates. For example,  $\text{Fe}_2\text{O}_3\text{-Cr}_2\text{O}_3$  and  $\text{Fe}_2\text{O}_3\text{-Cr}_2\text{O}_3\text{-NiO}$  films, which simulate passive films on ferritic and austenitic stainless steels, respectively, were formed on Pt substrates by MOCVD and their dissolution rates in acid solutions were examined as a function of film composition and applied potential.<sup>1-3</sup> The results showed that the dissolution rates of the films under cathodic polarization and open-circuit conditions decreased exponentially with increasing amount of  $\text{Cr}^{3+}$  cations.<sup>1-3</sup> Similar composition-dependent changes in the dissolution rate were found on real passive films on ferritic stainless steels, while the absolute dissolution rate of the real passive films was always higher than that of the artificial passivation films.<sup>1</sup> The other studies on sputter-deposited  $\text{Fe}_2\text{O}_3$ ,<sup>10</sup>  $\text{Cr}_2\text{O}_3$ ,<sup>11</sup> and  $\text{Fe}_2\text{O}_3\text{-Cr}_2\text{O}_3$ <sup>12,13</sup> thin films demonstrated that the reductive dissolution of  $\text{Fe}_2\text{O}_3$  and the oxidative dissolution of  $\text{Cr}_2\text{O}_3$  were suppressed by the presence of  $\text{Cr}_2\text{O}_3$  and  $\text{Fe}_2\text{O}_3$  in the films, respectively. It is noteworthy that the corrosion resistance does not vary linearly with film composition: even small amounts of a corrosion-resistant oxide component in the films can lead to a significant improvement of the corrosion resistance. In the case of  $\text{ZrO}_2\text{-Ta}_2\text{O}_5$ ,<sup>4</sup>  $\text{ZrO}_2\text{-TiO}_2$ ,<sup>5</sup> and  $\text{Fe}_2\text{O}_3\text{-TiO}_2$  films,<sup>6-8</sup> relatively small amounts of  $\text{Ta}_2\text{O}_5$  and  $\text{TiO}_2$  improve the corrosion resistance in strong acid solutions. The presence of  $\text{ZrO}_2$  in  $\text{Al}_2\text{O}_3\text{-ZrO}_2$  films<sup>9</sup> is effective in improving corrosion resistances in both acid and alkali solutions. The objective of the present work is to extend these studies to obtain  $\text{Al}_2\text{O}_3\text{-Ta}_2\text{O}_5$  double-oxide films having high corrosion resistances against both acid and alkali solutions.

The study on the corrosion resistance of  $\text{Al}_2\text{O}_3\text{-Ta}_2\text{O}_5$  thin films will also provide new insight into the passivity of Al-Ta alloys. In recent years there has been much interest in nonequilibrium solid-solution Al-Ta alloys prepared by sputter deposition, because the alloys show an excellent corrosion resistance in solutions containing chloride ions.<sup>14-19</sup> The pitting potential of a sputter-deposited Al-8 atom % Ta alloy in 0.1 M KCl at pH 7 is higher than that of pure Al by about 0.8 V.<sup>16</sup> Sputter-deposited Al-Ta alloys with about 40 atom % Ta behave like pure Ta, showing no pitting up to 1.6 V (vs. SCE) in 0.1 M NaCl at pH 10<sup>15</sup> and a negligibly small corrosion

rate in 1 M HCl.<sup>17,18</sup> In the present study we examined the corrosion resistance of  $\text{Al}_2\text{O}_3\text{-Ta}_2\text{O}_5$  films in HCl and NaOH solutions as a function of film composition. The results provide a better understanding of the passivation behavior of Al-Ta alloys in HCl solutions and give a clue to the mechanism responsible for the improved pitting resistance of the alloys in neutral chloride solutions.

## Experimental

**Synthesis of  $\text{Al}_2\text{O}_3\text{-Ta}_2\text{O}_5$  films.**— $\text{Al}_2\text{O}_3\text{-Ta}_2\text{O}_5$  films were prepared by MOCVD. Aluminum tetraisopropoxide [ $\text{Al}(\text{O}-i\text{-C}_3\text{H}_7)_3$ , 99.999 wt %] and tantalum pentametoxide [ $\text{Ta}(\text{OCH}_3)_5$ , 99.999 wt %] were employed as vapor sources and heated at 383 and 413 K, respectively. Nitrogen (99.999 vol %) was used as a carrier gas of each vapor source. The flow rate of carrier gas for each vapor source was changed in the range 0 to  $6.7 \times 10^{-6} \text{ m}^3 \text{ s}^{-1}$ , while the total flow rate of the carrier gases was kept constant at  $6.7 \times 10^{-6} \text{ m}^3 \text{ s}^{-1}$ . Oxygen (99.9 vol %) was used as a reactant gas and its flow rate was kept constant at  $8.3 \times 10^{-6} \text{ m}^3 \text{ s}^{-1}$ . The formation of the films was performed at a substrate temperature of 623 K. At this temperature, homogeneous amorphous  $\text{Al}_2\text{O}_3$  and  $\text{Ta}_2\text{O}_5$  films are deposited from  $\text{Al}(\text{O}-i\text{-C}_3\text{H}_7)_3$  and  $\text{Ta}(\text{OCH}_3)_5$ , respectively.<sup>20,21</sup>

Plates of polycrystalline Pt and single-crystal Si(100) in dimensions of  $25 \times 15 \times 0.5 \text{ mm}$  were used as substrates. The surface of the Pt plates was finished with 1  $\mu\text{m}$  diamond paste and degreased ultrasonically in acetone. Native oxide films on the Si(100) plates were removed by dipping in 2 wt % HF just before each experiment.

Figure 1 shows the schematic of the MOCVD system used. Source gases were evaporated in two evaporators and carried by the carrier gas. After the source gases were mixed with oxygen in a pipeline they were introduced into a cold wall CVD reactor. The tubing between the evaporators and the reactor was heated at 413 K to prevent the recondensation of source gases. The total pressure of the CVD reactor was kept at 2 kPa. The substrate was mounted on a holder with a built-in heater. Three baffle plates were used to get homogeneous gas flow. Two small square holes on a cover of the holder and two optical windows of the reactor cell allowed optical access to a substrate during the deposition under vacuum. The composition of the films was controlled by the flow rate of the carrier gas for each vapor source. The thickness of the films was adjusted to an appropriate value by monitoring the film growth and controlling the deposition time.

**Ellipsometric monitoring of film growth.**—A rotating analyzer ellipsometer was used to monitor the film formation in situ. The detail of the ellipsometer is described in the previous paper.<sup>9</sup> Briefly, monochromatic and linearly polarized light of wavelength 546.1 nm

\* Electrochemical Society Active Member.

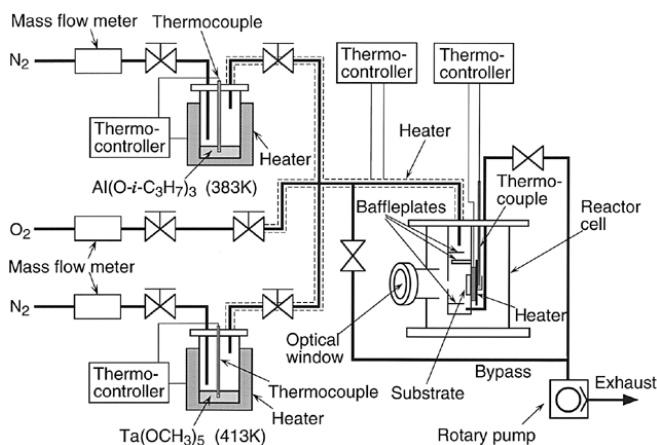


Figure 1. Schematic of MOCVD system.

was used as incident light and the angle of incidence was set at 60.00°. The intensity of light, which was reflected from the specimen surface and then passed through the rotating analyzer, was detected and digitized as a function of the angle of the analyzer by using a photodiode and related circuits. Computer-aided Fourier analysis of this signal provided two ellipsometric parameters, the relative phase retardation,  $\Delta$ , and the arc tangent of the relative amplitude reduction,  $\psi$ . The measured ellipsometric parameters can be related to the complex reflectance ratio<sup>22</sup> given by

$$\rho = R_p/R_s = \tan \Psi \cdot \exp(i\Delta) \quad [1]$$

where  $R_p$  and  $R_s$  are the complex amplitude reflection coefficients for light polarized parallel (p) and perpendicular (s) to the plane of incidence. The thickness and optical constants of deposited films were determined using a theoretical  $\Delta$  vs.  $\psi$  curve which fits the experimental data ( $\Delta$ ,  $\psi$ ) with minimal error. The theoretical  $\Delta$  vs.  $\psi$  curves were calculated using Drude's exact optical equations which express  $R_p$  and  $R_s$  for a three-medium (ambient-film-substrate) model.

**ICPS analysis.**—The chemical composition of oxide films was determined by chemical analysis. The oxide films deposited on the Si(100) plates were dissolved into 46 wt % HF solution of  $1 \times 10^{-5}$  m<sup>3</sup> volume and then the solution was diluted to  $5 \times 10^{-5}$  m<sup>3</sup> by adding distilled water. This diluted solution was analyzed by inductively coupled plasma-emission spectroscopy (ICPS). The results of ICPS analysis give the mass of Al and Ta in the films,  $W_{Al}$  and  $W_{Ta}$ . The cationic mole fraction of Ta in the film,  $X_{Ta}$ , was calculated from  $W_{Al}$  and  $W_{Ta}$  using the following equation

$$X_{Ta} = (W_{Ta}/M_{Ta}) / (W_{Al}/M_{Al} + W_{Ta}/M_{Ta}) \quad [2]$$

where  $M_{Al}$  and  $M_{Ta}$  are atomic weight of Al and Ta, respectively.

**XPS analysis.**—The chemical states of constituent elements of Al<sub>2</sub>O<sub>3</sub>-Ta<sub>2</sub>O<sub>5</sub> films deposited on Pt plates were analyzed by X-ray photoelectron spectroscopy (XPS). A Mg K $\alpha_{1,2}$  X-ray source (1253.1 eV) was operated at 5 kV and 30 mA. Photoelectron spectra of Al 2s, Ta 4d, O 1s, and C 1s levels were measured. The measurement of spectra was performed at a pressure of  $5 \times 10^{-5}$  Pa and at room temperature. For calibration of the photoelectron binding energy, the C 1s peak appearing at 285.0 eV in the background spectra was used. To examine chemical states and quantities of film constituent elements, measured spectra of O 1s and C 1s levels were approximated using the Gauss-Lorentz mixed function and those of Al 2s and Ta 4d levels were compared with the reference spectra taken from reagent-grade Al<sub>2</sub>O<sub>3</sub> and Ta<sub>2</sub>O<sub>5</sub> powder.

**Transmission electron microscopy observation.**—Micro- and crystal structures were examined by transmission electron microscopy (TEM) and electron diffraction (ED), respectively. Oxide films ca. 150 nm thick were deposited on KBr disks and then the disks were

dissolved by distilled water to separate the films. The separated films were picked by Cu mesh (180 mesh) and served for observation.

**Evaluation of corrosion resistance.**—The corrosion resistance of Al<sub>2</sub>O<sub>3</sub>-Ta<sub>2</sub>O<sub>5</sub> films formed on Pt substrates was examined in 6 and 12 M HCl and 1 M NaOH solutions at 298 K. After the films were immersed in the test solutions for a given time, the decrease in film thickness was measured by ellipsometry. Ellipsometric measurements were performed under the same conditions as described previously. The composition of the test solutions was analyzed by ICPS to examine the dissolved composition of the films. Before the ICPS analysis, 46 wt % HF solution of  $1 \times 10^{-6}$  m<sup>3</sup> volume was added to the test solution of  $4 \times 10^{-6}$  m<sup>3</sup> volume in order to dissolve Ta<sub>2</sub>O<sub>5</sub> groups, which may be detached from the films through the dissolution of Al<sub>2</sub>O<sub>3</sub>.

## Results and Discussion

**Ellipsometric analysis of the film formation process.**—Figure 2 illustrates the experimental  $\Delta$  vs.  $\Psi$  plots obtained during the deposition of Al<sub>2</sub>O<sub>3</sub>-Ta<sub>2</sub>O<sub>5</sub> films with  $X_{Ta}$  values of 0.16, 0.46, and 0.75. Solid lines in this figure indicate theoretical  $\Delta$  vs.  $\Psi$  curves calculated for the growth of films having different optical constants,  $N_2 = n_2 - k_2i$ . The experimental plot for the film of  $X_{Ta} = 0.16$  fits well the theoretical curve for  $N_2 = 1.51 - 0.00i$ , indicating no change in optical constants of the film during the deposition. Similarly, the experimental plots for the films of  $X_{Ta} = 0.46$  and 0.75 fit the theoretical curves calculated for the growth of films with  $N_2 = 1.66 - 0.00i$  and  $N_2 = 1.83 - 0.00i$ , respectively. The real part of optical constant  $N_2$ , i.e., refractive index  $n_2$ , of the film increases with increasing  $X_{Ta}$  value, while the imaginary part of  $N_2$ , i.e., extinction coefficient  $k_2$ , stays zero, indicating that films formed are optically transparent. From the fact that  $n_2$  values stay constant during the deposition of the films, it is suggested that the in-depth composition of the films is homogeneous. The ellipsometric monitoring of film growth allowed control of film thickness to a given value. In the experiments shown in Fig. 2, the supply of source gases was stopped when the film thickness reached  $\sim 80$  nm.

**Micro- and crystal structures.**—Figure 3 shows TEMs and ED patterns for Al<sub>2</sub>O<sub>3</sub>-Ta<sub>2</sub>O<sub>5</sub> films having different  $X_{Ta}$  values, which were formed at 623 K. All the films with  $X_{Ta}$  values between 0 and 1.0 have no crystal grains and show homogeneous structures. The ED patterns show unclear ring patterns, indicating that every film has an amorphous structure. It has been reported that CVD-Al<sub>2</sub>O<sub>3</sub><sup>20</sup> and Ta<sub>2</sub>O<sub>5</sub> films,<sup>21</sup> which are deposited at 523-773 K from Al(O-i-

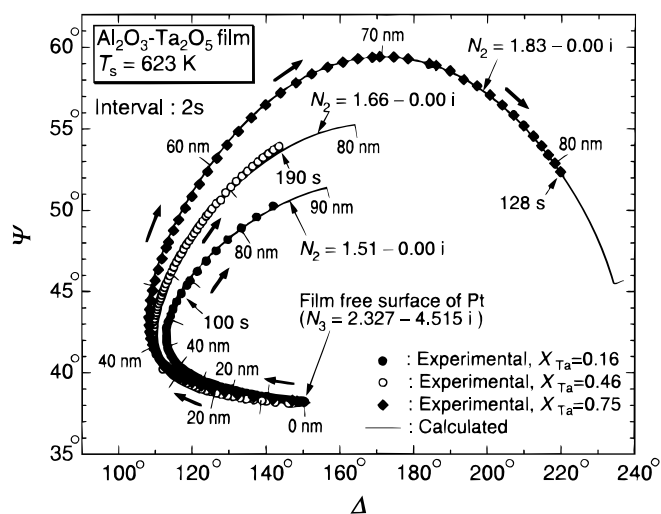


Figure 2. Experimental  $\Delta$ - $\Psi$  loci for formation of Al<sub>2</sub>O<sub>3</sub>-Ta<sub>2</sub>O<sub>5</sub> films and theoretical  $\Delta$ - $\Psi$  curves for growth of films with different optical constants,  $N_2 (=n_2 - k_2i)$ .

$C_3H_7)_3$  and at 473-773 K from  $Ta(OCH_3)_5$ , respectively, have an amorphous structure.

**Oxidation states of film constituent elements.**—Figure 4 shows XPS spectra of  $Al_2O_3$ - $Ta_2O_5$  films with different  $X_{Ta}$  values. The Al 2s spectra of the films exhibit a peak at  $119.3 \pm 0.1$  eV (Fig. 4a), and the Ta 4d spectra two peaks at  $230.7 \pm 0.1$  eV and  $242.4 \pm 0.1$  eV (Fig. 4b). The binding energies of these peaks are almost independent of  $X_{Ta}$  value. On the other hand, the peak energy of the O 1s spectrum shifts from 531.7 eV at  $X_{Ta} = 0.00$  ( $Al_2O_3$ ) to 531.0 eV at  $X_{Ta} = 1.00$  ( $Ta_2O_5$ ) with increasing  $X_{Ta}$  (Fig. 4c). The shift of the O 1s peak can be ascribed to the change in the  $OH^-/O^{2-}$  ratio of the films.

In Fig. 5a and b, the Al 2s and Ta 4d spectra for the  $Al_2O_3$ - $Ta_2O_5$  film with  $X_{Ta} = 0.19$  are compared with reference spectra from pure

$Al_2O_3$  and  $Ta_2O_5$ . Good coincidence between the measured and the reference spectra indicates that Al and Ta in the film exist as trivalent and pentavalent ions, respectively.

Figure 5c shows the decomposition of the O 1s spectrum for the  $Al_2O_3$ - $Ta_2O_5$  film with  $X_{Ta} = 0.19$ . The O 1s spectrum consists of contributions from three species having peaks at 531.10, 532.35, and 533.80 eV. The binding energies of these peaks are close to those for oxides ( $Al_2O_3$ : 530.95 eV,  $Ta_2O_5$ : 530.50 eV), a hydroxide ( $Al(OH)_3$ : 532.30 eV), and adsorbed  $H_2O$  (533.65-533.80 eV), respectively. Therefore, the oxygen species in the film are  $O^{2-}$ ,  $OH^-$ , and  $H_2O$ . The ratio of the peak area for  $OH^-$  species to that for  $O^{2-}$  species,  $S_{OH^-}/S_{O^{2-}}$ , depends on the film composition: the values of  $S_{OH^-}/S_{O^{2-}}$  for the films with  $X_{Ta} = 0.00, 0.18, 0.48,$  and  $1.00$  are 0.76, 0.54, 0.15, and 0.14, respectively. In the previous study using infrared spectroscopy, it has been demonstrated that CVD- $Al_2O_3$

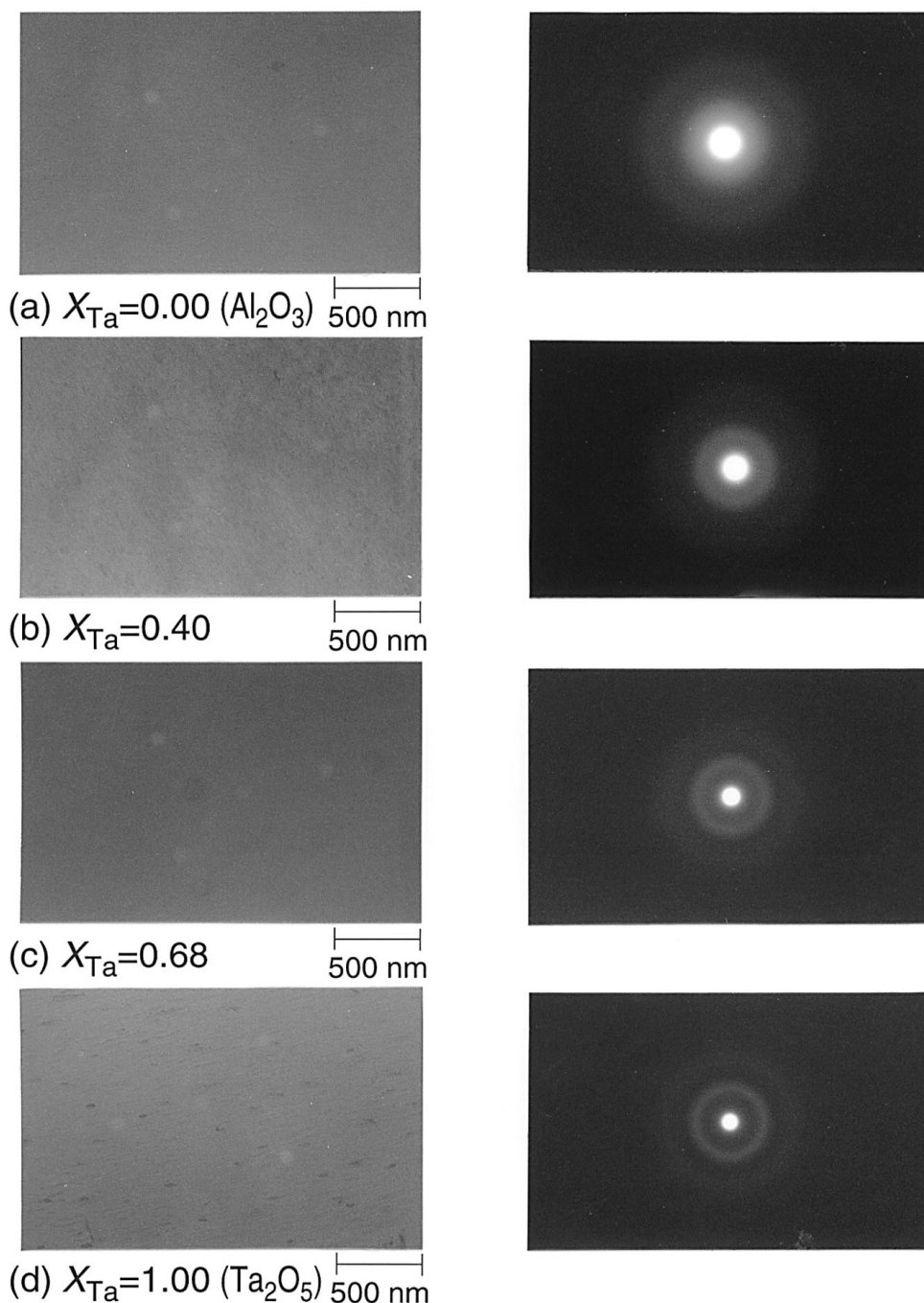


**Figure 3.** TEM (left) and ED patterns (right) for  $Al_2O_3$ - $Ta_2O_5$  films of  $X_{Ta} = 0.00$  ( $Al_2O_3$ ) (a), 0.40 (b), 0.68 (c), and 1.00 ( $Ta_2O_5$ ) (d).

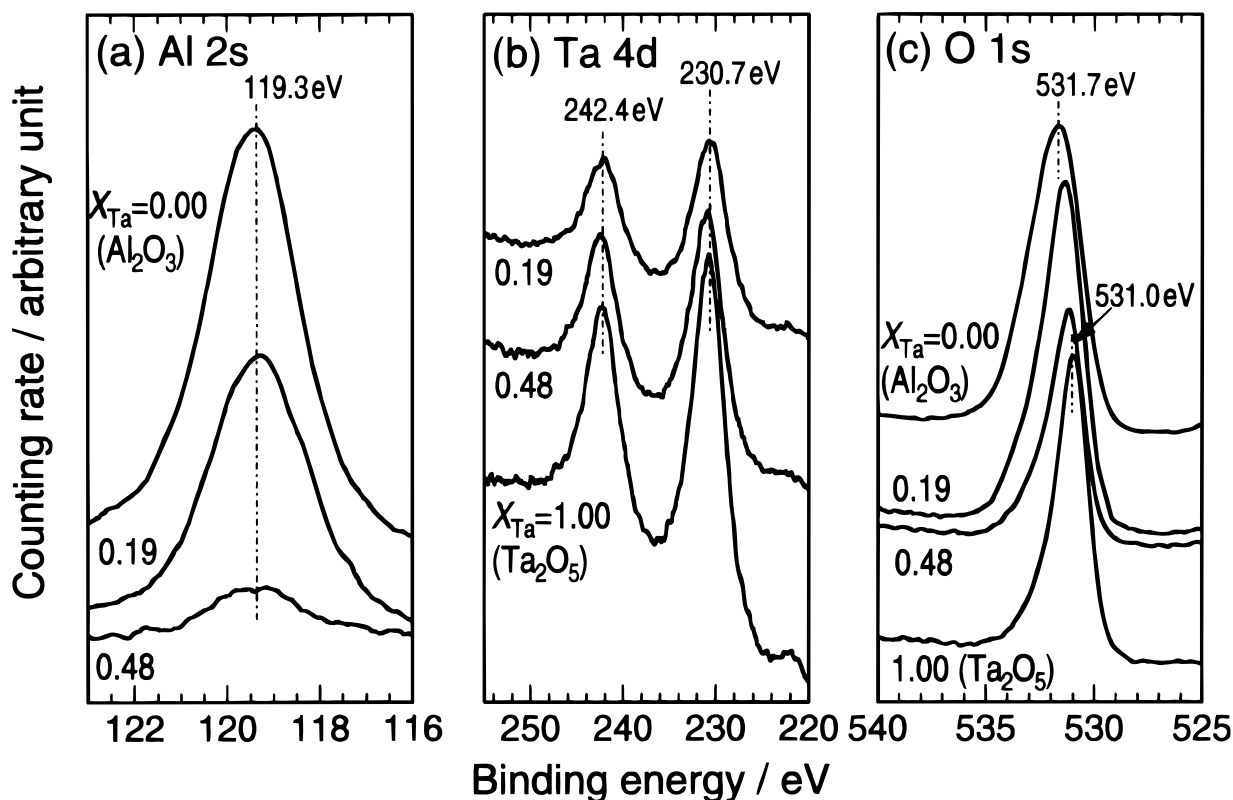


Figure 4. XPS spectra for  $\text{Al}_2\text{O}_3$ - $\text{Ta}_2\text{O}_5$  films deposited at 623 K.

films deposited from  $\text{Al}(\text{O}-i\text{-C}_3\text{H}_7)_3$  at 623 K had little or no Al-OH bond.<sup>20</sup> Therefore, hydroxyl groups detected by XPS may arise from adsorbed  $\text{OH}^-$  species on the surface of films, which is formed by water adsorption after the film formation.

*Corrosion resistance against HCl solution.*—Figure 6 illustrates changes in ellipsometric parameters,  $\Delta$  and  $\Psi$ , with immersion time for an  $\text{Al}_2\text{O}_3$ - $\text{Ta}_2\text{O}_5$  film of  $X_{\text{Ta}} = 0.12$  in 6 M HCl at 298 K. Theoretical  $\Delta$ - $\Psi$  curves calculated for the dissolution of films with dif-

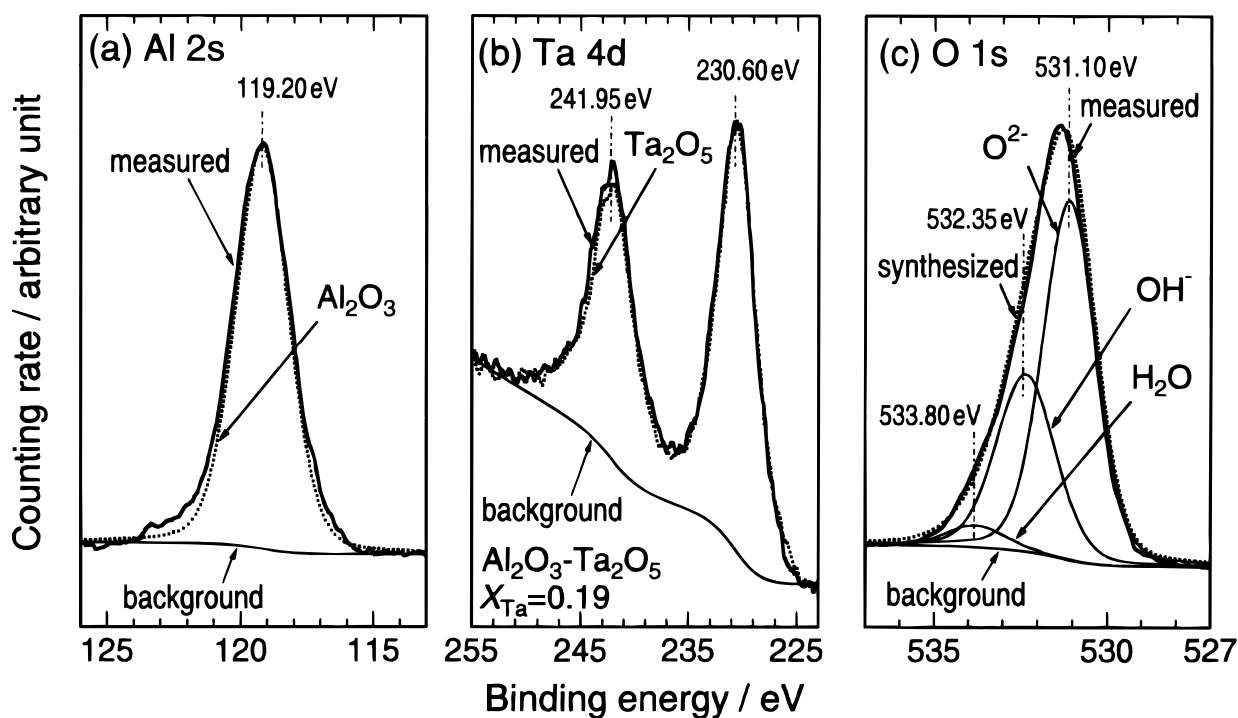
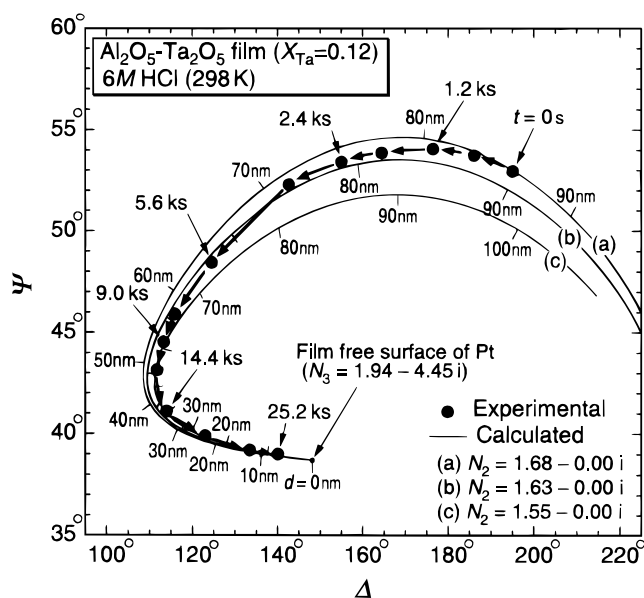


Figure 5. Comparison of Al 2s and Ta 4d spectra between  $\text{Al}_2\text{O}_3$ - $\text{Ta}_2\text{O}_5$  film of (a, b)  $X_{\text{Ta}} = 0.19$  and standard materials,  $\text{Al}_2\text{O}_3$  and  $\text{Ta}_2\text{O}_5$ , and (c) decomposition of O 1s spectrum of the film.

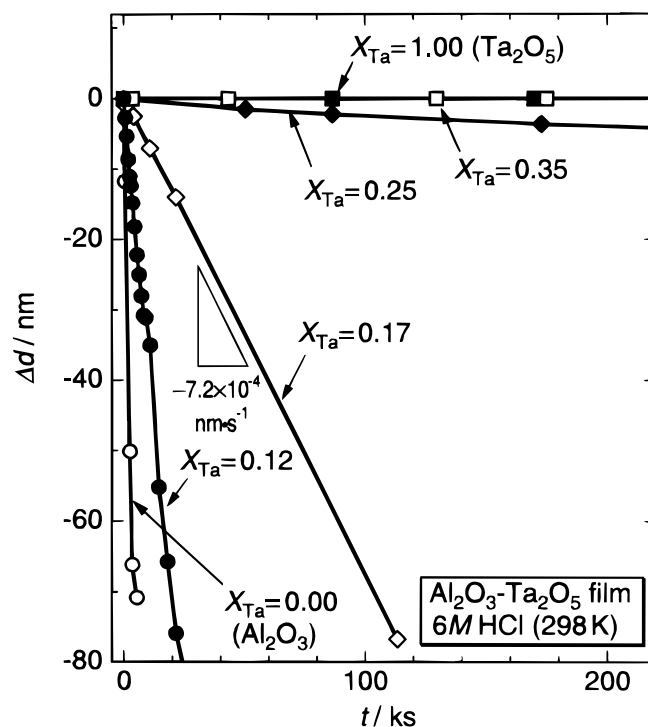
ferent optical constants,  $N_2 = n_2 - k_2i$ , are also given in Fig. 6. The experimental  $\Delta$ - $\Psi$  locus moves from a theoretical curve for a high optical constant,  $N_2 = 1.68 - 0.00i$ , to that for a low optical constant,  $N_2 = 1.55 - 0.00i$ . This decrease in the optical constant may be due to an increase in the surface roughness of the film with the progress of dissolution. A two-layer model, in which the film is assumed to consist of an outer rough layer and an inner compact layer, is better than a single, uniform layer model for determining the thickness changes during the dissolution. However, there are three or more unknown parameters in the two-layer model, and these parameters cannot be determined from two measured quantities,  $\Delta$  and  $\Psi$ . The following method was therefore employed to estimate the film thickness changes. First, an appropriate theoretical  $\Delta$  vs.  $\Psi$  curve which provides the best fit to the experimental ( $\Delta$ ,  $\Psi$ ) data through the whole test duration was searched. In the case of Fig. 6, the theoretical curve for the optical constant of  $N_2 = 1.63 - 0.00i$  was selected as the best fit curve. Then the thickness of the film remaining at each stage of dissolution was determined by drawing a perpendicular to the theoretical curve from the experimental plot. This method of film thickness determination leads to a small overestimation of the thickness of the film at the initial stage of dissolution. For the film at  $t = 0$  s in Fig. 6, the thickness determined using the theoretical curve for  $N_2 = 1.68 - 0.00i$ , which is the optical constant of as-formed film, is 85.5 nm; the thickness estimated using the theoretical curve for  $N_2 = 1.63 - 0.00i$ , which is the optical constant selected for the thickness analysis during the dissolution, is 89.5 nm. However, the error due to the overestimation never exceeded 5%.

Figure 7 shows the change in film thickness,  $\Delta d$ , in 6 M HCl at 298 K as a function of immersion time,  $t$ , for  $\text{Al}_2\text{O}_3$ - $\text{Ta}_2\text{O}_5$  films of  $X_{\text{Ta}} = 0.0 - 1.0$ . The thickness of the films with  $X_{\text{Ta}}$  values of 0.0-0.25 decreases linearly with time. One can determine the thinning rate of film thickness,  $-\Delta d/\Delta t$ , from the gradient of  $\Delta d$  vs.  $t$  curves.

The thinning rates thus determined are plotted against  $X_{\text{Ta}}$  in Fig. 8 where the corresponding results obtained in 12 M HCl at 298 K are also displayed. When the value of  $X_{\text{Ta}}$  exceeds about 0.1, the thinning rate of film thickness starts to decrease markedly with increasing  $X_{\text{Ta}}$  value. The  $X_{\text{Ta}}$  values at which the thinning rate reaches an analytical limit of ellipsometry,  $2.8 \times 10^{-6} \text{ nm s}^{-1}$ , are 0.35 and 0.45 in 6 and 12 M HCl solutions, respectively. The films having  $X_{\text{Ta}}$  values larger than 0.45 show superior corrosion resistance even in 12 M HCl at 298 K.



**Figure 6.** Experimental  $\Delta$ - $\Psi$  locus for dissolution of  $\text{Al}_2\text{O}_3$ - $\text{Ta}_2\text{O}_5$  film of  $X_{\text{Ta}} = 0.12$  in 6 M HCl at 298 K and theoretical  $\Delta$ - $\Psi$  curves for films with different optical constants,  $N_2$ .



**Figure 7.** Decrease in film thickness,  $\Delta d$ , as a function of time,  $t$ , for  $\text{Al}_2\text{O}_3$ - $\text{Ta}_2\text{O}_5$  films in 6 M HCl at 298 K.

To examine whether the selective dissolution of film constituent elements occurs, the amount of metal ions dissolved in the test solution was measured by ICPS. Figure 9 exhibits the amount of dissolved Al and Ta ions,  $W_{\text{Al}}$  and  $W_{\text{Ta}}$ , as a function of the exposure time,  $t$ , for the  $\text{Al}_2\text{O}_3$ - $\text{Ta}_2\text{O}_5$  film of  $X_{\text{Ta}} = 0.25$  in 6 M HCl at 298 K.

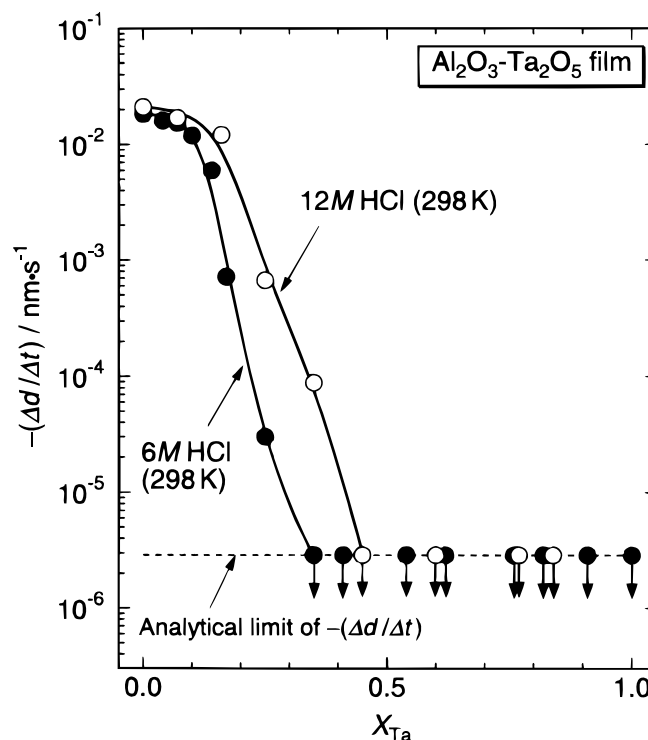


**Figure 8.** Thinning rate of film thickness,  $-\Delta d/\Delta t$ , as a function of cationic mole fraction of Ta,  $X_{\text{Ta}}$ , for  $\text{Al}_2\text{O}_3$ - $\text{Ta}_2\text{O}_5$  films in 6 M HCl and 12 M HCl at 298 K.

The dashed curve in Fig. 9 indicates the  $W_{Al}$  vs.  $t$  curve calculated from the experimental  $W_{Ta}$  vs.  $t$  curve under the assumption that no selective dissolution occurs. The experimental  $W_{Al}$  values are about three times the calculated ones, indicating that the selective dissolution of  $Al^{3+}$  ions takes place during the immersion. The selective dissolution of  $Al^{3+}$  ions probably produces a porous or rough surface layer, where  $Ta_2O_5$  is enriched, in the surface region of residual films. As a result, the optical constants of  $Al_2O_3$ - $Ta_2O_5$  films change with immersion time (Fig. 6). Under the assumption that a rough surface layer is optically equivalent to a mixture of oxides and voids, the refractive index of the surface layer,  $n_s$ , is given as a function of the refractive indices of oxides and voids,  $n_{ox}$  and  $n_v$  ( $=1$ ), and the volume fractions of these components,  $f_{ox}$  and  $f_v$  ( $=1 - f_{ox}$ ). As expected from Fig. 2,  $n_{ox}$  increases as  $Ta_2O_5$  is enriched by the selective dissolution of Al, which would result in an increase in  $n_s$  if there is little or no surface roughening ( $f_v \approx 0$ ).  $n_s$  is expected to decrease when the dissolution of  $Al_2O_3$ - $Ta_2O_5$  films is followed by significant surface roughening ( $f_v > 0$ ). A decrease in  $n_s$  leads to a decrease in averaged optical constants of the films remaining at each stage of dissolution. The observed decrease in optical constants with time (Fig. 6) should show that the surface of the films becomes rough in the progress of dissolution.

**Corrosion resistance against NaOH solution.**—Changes in the ellipsometric parameters during the dissolution of  $Al_2O_3$ - $Ta_2O_5$  films in 1 M NaOH were similar to those observed in 6 M HCl (Fig. 6). Figure 10 shows the change in film thickness,  $\Delta d$ , in 1 M NaOH at 298 K as a function of immersion time,  $t$ , for  $Al_2O_3$ - $Ta_2O_5$  films of  $X_{Ta} = 0.0 - 1.0$ . The thickness of the films with  $X_{Ta}$  values of 0.0-0.53 decreases linearly with time. The thinning rate of film thickness,  $-\Delta d/\Delta t$ , for each film was determined from the gradient of the corresponding  $\Delta d$  vs.  $t$  curve.

Figure 11 shows the thinning rates of film thickness for  $Al_2O_3$ - $Ta_2O_5$  films in 1 M NaOH at 298 K as a function of  $X_{Ta}$ . In 1 M NaOH, the film with  $X_{Ta} = 0.0$  ( $Al_2O_3$ ) is very susceptible to corrosion, because the thinning rate in this solution is higher than that in 6 M HCl by a factor of 1,000. The thinning rate of the  $Al_2O_3$ - $Ta_2O_5$  films, however, decreases significantly with increasing  $X_{Ta}$ , and at  $X_{Ta}$  values larger than 0.5 it becomes six orders of magnitude lower than that of the film with  $X_{Ta} = 0.0$  ( $Al_2O_3$ ). The films with  $X_{Ta}$  values larger than 0.5 behave like pure  $Ta_2O_5$  film. Taking account of the results obtained in HCl solutions, it is concluded that the  $Al_2O_3$ -

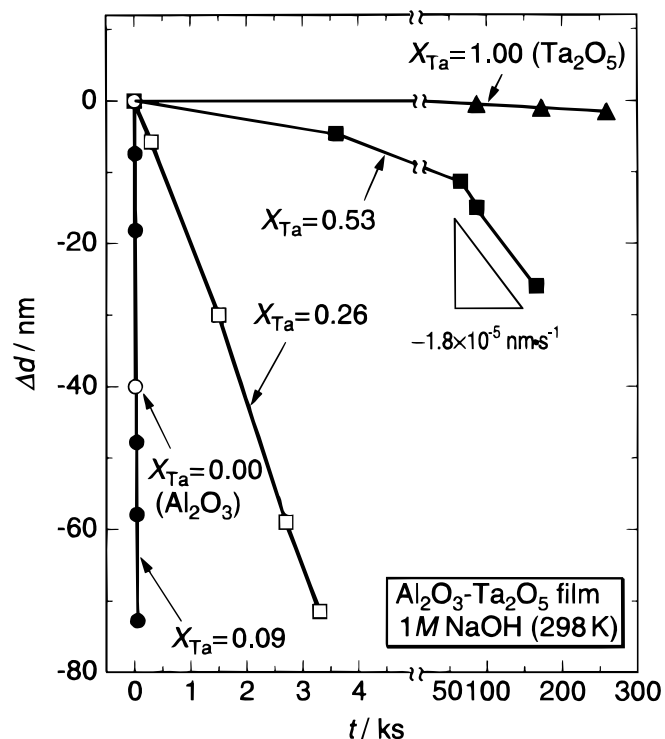


Figure 10. Decrease in film thickness,  $\Delta d$ , as a function of time,  $t$ , for  $Al_2O_3$ - $Ta_2O_5$  films in 1 M NaOH at 298 K.

$Ta_2O_5$  double-oxide films with  $X_{Ta}$  values larger than 0.5 have excellent corrosion resistance against both the acid and alkali solutions.

**Insight into passivity and its breakdown of Al-Ta alloys.**—It has been reported that sputter-deposited Al-Ta alloys containing more than 14 atom % Ta passivate spontaneously in 1 M HCl at 303 K.<sup>14</sup>

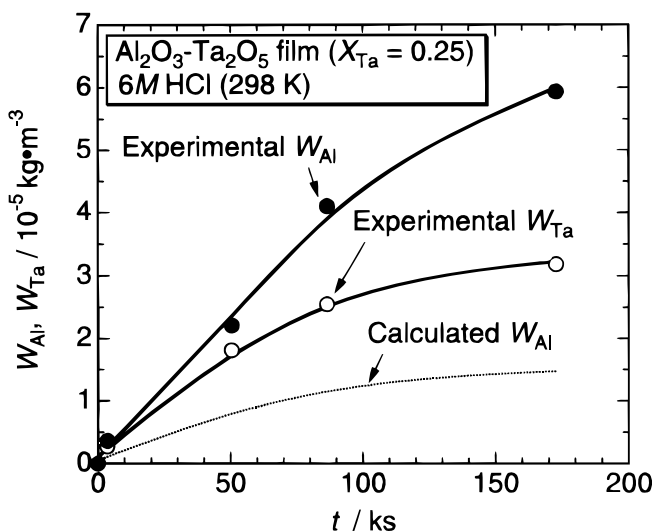


Figure 9. Amount of dissolved Al and Ta ions,  $W_{Al}$  and  $W_{Ta}$ , as a function of time,  $t$ , for  $Al_2O_3$ - $Ta_2O_5$  film of  $X_{Ta} = 0.25$  in 6 M HCl at 298 K. Dashed curve indicates  $W_{Al}$  vs.  $t$  relationship calculated by assuming uniform (nonselective) dissolution of the film.

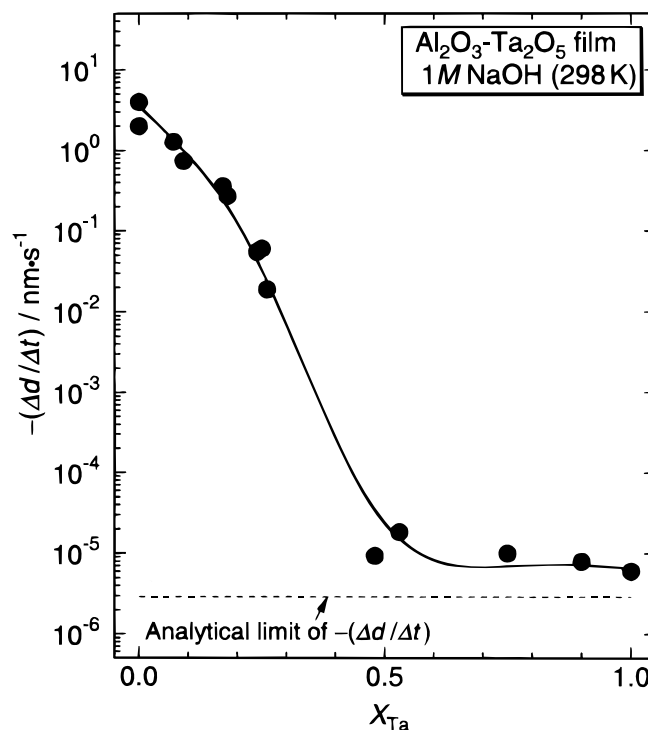


Figure 11. Thinning rate of film thickness,  $-\Delta d/\Delta t$ , as a function of cationic fraction of Ta,  $X_{Ta}$ , for  $Al_2O_3$ - $Ta_2O_5$  films in 1 M NaOH at 298 K.

As a result, the corrosion rate of the alloys decreases significantly with increasing Ta content, and the alloy containing 53 atom % Ta hardly dissolves in 1 M HCl at 303 K.<sup>17,18</sup> The results of XPS analysis showed that the fraction of Ta<sup>5+</sup> in the passive films formed in 1 M HCl is almost the same as that of Ta in the alloys.<sup>14</sup> These observations agree with the results obtained in the present study: Fig. 8 reveals that double-oxide films consisting of Al<sup>3+</sup> and Ta<sup>5+</sup> cations become protective with increasing Ta<sup>5+</sup> fraction,  $X_{Ta}$ , and the films with  $X_{Ta}$  values of about 0.45 are immune to corrosion even in concentrated HCl solutions.

The pitting potential of sputter-deposited Al–Ta alloys in neutral chloride solutions increases with increasing Ta content of the alloys.<sup>15,16,19</sup> Several mechanisms have been proposed to explain the improved pitting resistance of Al–Ta alloys. Davis et al.<sup>16</sup> found, using XPS, that the passive film on Al–Ta alloys is enriched in Ta<sub>2</sub>O<sub>5</sub>. They proposed that the Ta<sub>2</sub>O<sub>5</sub>-rich passive film resists the Cl<sup>-</sup> penetration through the film, improving the resistance to pitting corrosion.<sup>16</sup> Natishan et al.<sup>23</sup> proposed that the enrichment of Ta<sub>2</sub>O<sub>5</sub> in the passive film decreases the pH of zero charge of the film, inhibiting the adsorption of Cl<sup>-</sup> and thus enhancing the pitting resistance. On the other hand, Smialowska<sup>24</sup> and Frankel et al.<sup>25</sup> suggested that the alloying elements in Al-transition metal alloys exert their influences at active pits rather than passive films. Smialowska<sup>24</sup> proposed that in the case of Al–Cr, Al–Zr, and Al–W alloys, the low solubility of oxidized alloying elements, CrOOH, ZrO<sub>2</sub>, and WO<sub>3</sub>, in an acidified micropit impedes pit propagation. Frankel et al.<sup>25</sup> suggested that alloying elements such as Nb and Mo reduce the ability of micropits to maintain the critical environment necessary for growth. As can be seen in Fig. 8, the dissolution rate of Al<sub>2</sub>O<sub>3</sub>–Ta<sub>2</sub>O<sub>5</sub> films in HCl solutions, which correspond to acidic micropit environments, decreases markedly with increasing Ta<sup>5+</sup> content of the films. It is at least suggested that the repassivation ability of Al–Ta alloys in acidic micropit environments increases significantly with increasing Ta content of the alloys, even though the unique mechanism responsible for the improved pitting resistance of the alloys cannot be conclusively determined from these results.

### Conclusions

1. Al<sub>2</sub>O<sub>3</sub>–Ta<sub>2</sub>O<sub>5</sub> double-oxide films having different cationic fraction of Ta,  $X_{Ta}$ , were formed at 623 K by MOCVD using Al(O–*i*-C<sub>3</sub>H<sub>7</sub>)<sub>3</sub> and Ta(OCH<sub>3</sub>)<sub>5</sub> as source gases.

2. The Al<sub>2</sub>O<sub>3</sub>–Ta<sub>2</sub>O<sub>5</sub> films having  $X_{Ta}$  values between 0.0 and 1.0 showed homogeneous amorphous structures. Aluminum, tantalum, and oxygen in the films existed in the state of Al<sup>3+</sup>, Ta<sup>5+</sup>, and O<sup>2-</sup> ions. In the surface region of Al<sub>2</sub>O<sub>3</sub>-rich films, oxygen existed also as OH<sup>-</sup> ions.

3. The thinning rate of the Al<sub>2</sub>O<sub>3</sub>–Ta<sub>2</sub>O<sub>5</sub> films in HCl solutions decreased with increasing  $X_{Ta}$  value. The films with  $X_{Ta}$  values of

0.35 and 0.45 exhibited superior corrosion resistance against 6 M HCl and 12 M HCl solutions at 298 K, respectively.

4. The thinning rate of the Al<sub>2</sub>O<sub>3</sub>–Ta<sub>2</sub>O<sub>5</sub> films in 1 M NaOH decreased significantly with increasing  $X_{Ta}$  value and at  $X_{Ta}$  larger than 0.5 it becomes six orders of magnitude lower than that of pure Al<sub>2</sub>O<sub>3</sub> film.

Tohoku University assisted in meeting the publication costs of this article.

### References

1. K. Sugimoto, M. Seto, S. Tanaka, and N. Hara, *J. Electrochem. Soc.*, **140**, 1586 (1993).
2. S. Tanaka, N. Hara, and K. Sugimoto, in *Corrosion Protection by Coatings and Surface Modification*, M. W. Kendig, K. Sugimoto, and N. R. Soerensen, Editors, PV 93-28, p. 54, The Electrochemical Society Proceedings Series, Pennington, NJ (1993).
3. S. Tanaka, N. Hara, and K. Sugimoto, *Mater. Sci. Eng.*, **A198**, 63 (1995).
4. K. Amano and K. Sugimoto, *J. Jpn. Inst. Metals*, **56**, 1192 (1992).
5. S. Kikkawa, N. Hara, and K. Sugimoto, *Mater. Sci. Forum*, **185-188**, 497 (1995).
6. K. Sugimoto, H. Kim, N. Akao, and N. Hara, in *Surface Oxide Films*, J. A. Bardwell, Editor, PV 96-18, The Electrochemical Society Proceedings Series, p. 195, Pennington, NJ (1996).
7. H. Kim, N. Hara, and K. Sugimoto, *J. Electrochem. Soc.*, To be published.
8. H. Kim, N. Akao, N. Hara, and K. Sugimoto, *J. Electrochem. Soc.*, **145**, 2818 (1998).
9. E. Takahashi, N. Akao, N. Hara, and K. Sugimoto, in *Organic and Inorganic Coatings for Corrosion Prevention-Research and Experiences*, L. Fedrizzi and P. L. Bonora, Editors, p. 299, The Institute of Materials, London (1996).
10. S. Virtanen, P. Schmuki, A. J. Davenport, and C. M. Vitus, *J. Electrochem. Soc.*, **144**, 198 (1997).
11. P. Schmuki, S. Virtanen, A. J. Davenport, and C. M. Vitus, *J. Electrochem. Soc.*, **143**, 3997 (1996).
12. P. Schmuki, S. Virtanen, H. Böhni, H. S. Isaacs, and A. J. Davenport, in *Surface Oxide Films*, J. A. Bardwell, Editor, PV 96-18, The Electrochemical Society Proceedings Series, p. 234, Pennington, NJ (1996).
13. P. Schmuki, S. Virtanen, H. S. Isaacs, M. P. Ryan, A. J. Davenport, H. Böhni, and T. Stenberg, *J. Electrochem. Soc.*, **145**, 791 (1998).
14. H. Yoshioka, A. Kawashima, K. Asami, and K. Hashimoto, in *Corrosion, Electrochemistry and Catalysis of Metallic Glasses*, R. B. Diegle and K. Hashimoto, Editors, p. 242, The Electrochemical Society, Pennington, NJ (1988).
15. G. S. Frankel, M. A. Russak, C. V. Jahnes, M. Mirzamaani, and V. A. Brusica, *J. Electrochem. Soc.*, **136**, 1243 (1989).
16. G. D. Davis, W. C. Moshier, T. L. Fritz, and G. O. Gote, *J. Electrochem. Soc.*, **137**, 422 (1990).
17. H. Yoshioka, Q. Yan, H. Habazaki, A. Kawashima, K. Asami, and K. Hashimoto, *Corros. Sci.*, **31**, 349 (1990).
18. K. Hashimoto, N. Kumagai, H. Yoshioka, H. Habazaki, A. Kawashima, K. Asami, and B.-P. Zhang, *Mater. Sci. Eng.*, **A133**, 22 (1991).
19. C. C. Streinz, J. Kruger, and P. J. Moran, *J. Electrochem. Soc.*, **141**, 1126 (1994).
20. T. Go and K. Sugimoto, *J. Jpn. Inst. Metals*, **56**, 184 (1992).
21. C. H. An and K. Sugimoto, *J. Electrochem. Soc.*, **139**, 1956 (1992).
22. R. M. A. A. Azzam and N. M. Bashara, *Ellipsometry and Polarized Light*, North-Holland, New York (1979).
23. P. M. Natishan, E. McCafferty, and G. K. Hubler, *J. Electrochem. Soc.*, **135**, 321 (1988).
24. Z. Szklarska-Smialowska, *Corros. Sci.*, **33**, 1193 (1992).
25. G. S. Frankel, R. C. Newman, C. V. Jahnes, and M. A. Russak, *J. Electrochem. Soc.*, **140**, 2192 (1993).